Probing the in-depth distribution of organic/inorganic molecular species within the SEI of LTO/NMC and LTO/LMO batteries: A complementary ToF-SIMS and XPS study

Nicolas Gauthier, Cecile Courreges, Julien Demeaux, Cécile Tessier, Hervé Martinez

Probing the in-depth distribution of organic/inorganic molecular species within the SEI of LTO/NMC and LTO/LMO batteries: a complementary ToF-SIMS and XPS study.

Nicolas Gauthier[1,2], *Cécile Courrèges*[1,*], *Julien Demeaux*[2], *Cécile Tessier*[2], *and Hervé Martinez*[1,3]

[1]CNRS/ UNIV Pau & Pays Adour/ E2S UPPA, Institut des Sciences Analytiques et de Physicochimie pour l'Environnement et les Matériaux, UMR5254, 64000, Pau, France

[2]SAFT, 111-113 Boulevard Alfred Daney, 33000 Bordeaux, France

[3]Réseau sur le Stockage Electrochimique de l'Energie (RS2E), CNRS FR3459, 33 Rue Saint Leu, 80039 Amiens Cedex, France

Corresponding Author

*Cécile Courrèges

cecile.courreges@univ-pau.fr

ABSTRACT

Spinel $Li_4Ti_5O_{12}$ (LTO) is an attractive candidate for negative electrode materials of Li-ion batteries because of its outstanding safety characteristics. In this paper, the influence of common high voltage cathodes, $LiNi_{3/5}Co_{1/5}Mn_{1/5}O_2$ (NMC) and $LiMn_2O_4$ (LMO), upon the electrochemical performances of LTO/LMO and LTO/NMC cells, in relation with the Solid

Electrolyte Interphase (SEI) properties formed over the LTO surface, is studied. After cycling, the electrodes were analyzed by ToF-SIMS and XPS with two X-ray sources (Ag and Al) to investigate both the chemical composition and the in-depth distribution of specific SEI species at the electrode surface. Facing both counter-electrodes, LTO electrodes are covered by surface layers due to the degradation of electrolyte components inducing an irreversible capacity loss, more important for LTO/LMO cells. The chemical composition of both layers is similar: organic and inorganic species but the SEI formed on LTO electrode cycled facing LMO electrode is thicker and contains small amounts of manganese compounds from the positive electrode. Moreover, 3D mappings reconstructed from ToF-SIMS depth-profile experiments, display different in-depth spatial distributions of SEI species, which are in agreement with XPS results. Consequently, the impact of interactions between electrodes on the formation of surface films is discussed.

KEYWORDS: Li-ion Batteries, SEI, $Li_4Ti_5O_{12}$ (LTO), $LiN_{3/5}iCo_{1/5}Mn_{1/5}O_2$ (NMC), $LiMn_2O_4$ (LMO), ToF-SIMS, depth-profiles, XPS (Al and Ag sources).

1. INTRODUCTION

Li-ion batteries are widely used nowadays for electric energy storage such as in electric vehicles which have increased the demand and the requirements in terms of voltage and safety[1,2]. Their electrochemical performances rely on the intrinsic properties of the active materials and on the electrode/electrolyte interfaces. Thus, the formation of a stable surface layer (5-10 nm), called "Solid Electrolyte Interphase" (SEI) plays a major role in Li-ion batteries working. This SEI is composed of solvent and lithium salt degradation products and should ensure the passivation of the electrode surface while maintaining an efficient diffusion of lithium ions[3,4]. For high current densities, carbon-based anodes, are associated with the risk

of lithium plating and dendrites formation, which presents a real safety hazard. In this context, other active materials, such as lithium titanate $Li_4Ti_5O_{12}$ (LTO), have been considered and extensively studied. Indeed, LTO presents interesting characteristics with a high plateau intercalating potential of 1.55 V vs Li^+/Li^0, avoiding any dendrite plating [5,6], and a negligible change of lattice parameter during Li^+ insertion/extraction, resulting in a very low capacity decrease upon cycling[7,8]. Nevertheless, different studies have shown the formation of a SEI (composed of LiF, fluorophosphates, alkylcarbonates, oxalates, ethylene oxides) and gassing occurring at the LTO electrode surface at different temperatures in half and full cells, which can affect cell electrochemical performances[9-15]. In addition, even if the high working potential of spinel LTO renders the system safer, it is at the cost of a loss of energy density. Consequently, the LTO implementation requires the use of high voltage cathodes such as layered metal oxide $LiNi_{3/5}Co_{1/5}Mn_{1/5}O_2$ (NMC) electrode[16] and spinel oxide $LiMn_2O_4$ (LMO) electrode[6,17], which are commonly used until 4V. However, the manganese-based materials exhibit transition metal dissolution in the electrolyte during cycling and deposition on the negative electrode surface, identified as a potential issue for batteries cycle life[18-21]. In a previous study, we showed that LTO/NMC full cell cycled at 3.0V presents better electrochemical performances over the first hundred cycles compared to the LTO/LMO system cycled at 3.2V[22]. Indeed, the capacity becomes stable faster for LTO/NMC and remains higher (147±3 $mAh.g^{-1}$ after 100 cycles) compared to LTO/LMO (140±3 $mAh.g^{-1}$ after 100 cycles). These electrochemical results were correlated with the formation and the evolution of both LTO electrode/electrolyte interface layers cycled against NMC or LMO electrodes by X-ray Photoelectron Spectroscopy (XPS) and Scanning Auger Microscopy (SAM) measurements. XPS analysis quantitatively evidenced that the SEI formed on the LTO electrode cycled facing LMO is thicker than the one formed facing NMC electrode. Besides, the SEI formed on the LTO electrode surface vs LMO contains small amounts of manganese compounds (detected by XPS), homogeneously spread over the surface, as revealed by SAM.

Thanks to its high sensitivity and in-depth resolution (< 1 nm), ToF-SIMS can also be very useful to characterize the in-depth distribution of molecular SEI species, through sputter-depth-profiling experiments. For instance, the accumulation of manganese at the graphite electrode surface has already been observed by secondary ion mass spectrometry[23]. Moreover, the surface of graphite and lithium electrodes have been analyzed by ToF-SIMS and the formation of a surface layer, where the organic products are mostly located in the outer part, has been observed[24, 25].

The objective of the present work is to characterize the in-depth spatial distribution of SEI species at the LTO electrode surface over cycling by coupling ToF-SIMS (surface and depth-profile experiments) and XPS using two different sources (Al: 1486.6 eV and Ag: 284.3 eV with a depth of analysis of 5-10 nm and 10-20 nm respectively). The deposition of manganese species at the LTO electrode surface is particularly followed. Moreover, the interactions between the two electrodes during cycling are investigated, which can directly influence on the capacity and the stability of cells. Finally, the in-depth spatial distribution of inorganic and organic SEI molecular species upon cycling is reported for the first time to better understand the SEI impact at the LTO electrode surface on batteries electrochemical performances.

2. EXPERIMENTAL SECTION

2.1 Cell preparation and cycling protocol

The electrodes formulation requires first the preparation of an ink which is then coated on a current collector (in aluminum), calendered and then dried (100°C under vacuum for 12 h to remove residual water). To prepare this ink, 93 wt% of anhydrous active material (LTO, NMC or LMO) supplied by SAFT, 4 wt% of carbon black (CB) as additive with a specific surface of 65 $m^2.g^{-1}$, (99.8% purity) Super C65 TIMCAL from Alfa Aesar, and 3 wt% of

poly(vinylidene fluoride) (PVdF) used as polymeric binder, supplied by Solvay (Solef 5130), are mixed together using a T25 digital ULTRA-TURRAX homogenizer. Note that the electrodes are prepared so that they are limited by the LTO negative electrode active mass. The liquid electrolyte is a mixture of ethylene carbonate (EC) and ethylmethyl carbonate (EMC) (3:7 in volume), containing $LiPF_6$ as lithium salt (1 $mol.L^{-1}$) from BASF (battery grade) with a water content <50 ppm. Coin cells are assembled in an argon-filled glove box using 0.25 ml of electrolyte and two polypropylene (Celgard) separators. Using a MPG2 battery cycler (Biologic SA, Claix, France), cells are cycled at 60°C (in a thermostatic oven) under galvanostatic mode at C/10 rate from open circuit voltage for the first cycle, and at 40°C under galvanostatic mode at C/2 rate (based on the LTO theoretical capacity, 175 $mAh.g^{-1}$) for the next hundred cycles. Full-cells cycling experiments are controlled in order to cycle LTO electrode between 1,0 V and 2,0 V: NMC/LTO cells are then cycled between 1,9 V and 3,0 V and LMO/LTO cells between 2,0 V and 3,1 V. After cycling, coin cells are opened in an argon-filled glove box (<1 ppm H_2O and O_2) and all LTO, NMC and LMO electrodes are extracted and washed with 1.0 ml of DMC for 30 s in a beaker to remove residus of electrolyte. Note that the washing procedure (which can partially dissolve species deposited at the electrode surface) was strictly the same for all samples so that the results are comparable.

2.2 Surface Analyses

Time-of-Flight Secondary Ion Mass Spectrometry (ToF-SIMS). ToF-SIMS analysis are performed using a TRIFT V nanoToF II (Physical Electronics, Chanhassen (MN), US) equipped with a 30 kV Au-LMIG. The electrode samples are fixed with a metallic mask on the sample holder and transferred from the gloves box to the spectrometer using a transfer vessel to avoid any air exposure. For surface analysis, all mass spectra are acquired using the same experimental conditions which allow performing semi-quantitative analysis (comparing

the ratio of peaks intensities): the LMIG gun is tuned to deliver Au^+ primary ions with a DC current of 12 nA over a 50x50 μm^2 raster size, the mass range is fixed between 0 and 800 um and the number of frames is set to 30 (dose: $5x10^{13}$ ions/cm^2) for both positive and negative polarities. Depth profile experiments (series of 30 cycles "analysis/sputtering") are carried out using the previous conditions for surface analysis (Au^+, 50x50μm^2 raster size) and a 5 kV Ar^+ gas gun for etching (with an etching time of 20 seconds for each cycle, a DC current of 300 nA and a sputtered area of 500x500 μm^2). Note that the lithium ($^6Li^+$ and $^7Li^+$) peaks appear very intense and have to be blanked during the measurement so that to detect better the smaller peaks. Data processing is performed using ToF-DR software provided by Physical Electronics. All positive polarity mass spectra are calibrated using K^+ (m/z 39), Ti^+(m/z 55) and TiO^+(m/z 64) peaks and all negative polarity spectra are calibrated using F^- (m/z 19), O^- (m/z 16) and P^- (m/z 31) peaks.

X-ray Photoelectron Spectroscopy (XPS). XPS are carried out using an Escalab 250 Xi spectrometer (Thermo Fischer Scientific, Waltham (Massachusetts), US) equipped with two monochromatized sources, either Al Kα (hν =1486.6 eV) or Ag Lα (hν = 2984.3 eV). Electrode samples are put on a sample holder using a metallic clamp and transferred through an argon-filled glove box with low H_2O/O_2 levels (< 5 ppm) directly connected to the spectrometer in order to prevent any moisture/air contamination. High resolved spectra are recorded using constant 20 eV and 200 eV pass energies for Al and Ag sources respectively. Analyses are performed using a 0.15 eV step size and short time iterative scans to follow any sample degradation. Only "non degraded" spectra are taken in account and summed for data treatment with CasaXPS software. For spectral calibration, the CF_2 component (at 290.7eV) from the PVdF binder in C 1s core peak is considered, as the hydrocarbon and carbon black binding energy (~ at 285eV) can be shifted due to the presence of SEI species containing C-C/C-H and due to the lithiation state of the electrode [12, 13, 22]. Peak fitting is processed with a non-linear

Shirley-type background and the peak deconvolution is obtained with a weighted least-squares calculation method using 30% Lorentzian and 70% Gaussian line shapes and full width at half maximum (fwhm) constraints.

3. RESULTS AND DISCUSSION

3.1 ToF-SIMS analysis

3.1.1 References and Pristine electrode

To make the interpretation of ToF-SIMS data easier, reference compounds from the electrolyte and the electrodes were first analyzed separately in order to establish a database with the main specific secondary ions for each species both in positive and negative polarities. Only positive spectra are shown in this paper as they present the peaks of interest for our study. Therefore, relevant compounds like LTO-powder active material, PVdF binder, carbon additives, $LiPF_6$ electrolyte salt and LiF were analyzed. Table 1 displays a list of the main peaks detected over a 0-100 m/z range for these compounds in the positive polarity.

LTO Powder		**Reference PVdF**		**Reference CB**		**References $LiPF_6$/LiF**		**Reference Li_2CO_3**	
m/z	**ID**	**m/z**	**ID**	**m/z**	**ID**	**m/z**	**ID**	**m/z**	**ID**
7	Li	12	C	13	CH	14	Li_2		
27	C_2H_3	31	CF	14	CH_2	19	F		
30	Li_2O	41	H_3F_2	15	CH_3			30	Li_2O
39	K	43	C_3H_3O	26	C_2H_2	33	Li_2F	31	Li_2OH
48	Ti	51	CHF_2	27	C_2H_3	59	Li_3F_2	37	Li_3O
64	TiO	69	CF_3	29					
97	TiO_3H	77	$C_3H_3F_2$		C_2H_5	85	Li_4F_3	81	Li_3CO_3

Table 1. Main secondary ions detected by ToF-SIMS for references powders (LTO, PVdF, CB, $LiPF_6$/LiF, Li_2CO_3) over a 0-100 m/z range in the positive polarity (ID stands for identification).

Moreover, LTO pristine electrode was analyzed before cycled electrodes; the ToF-SIMS spectrum collected in the positive polarity in the 0-100 m/z range is presented in figure 1. A large number of fragments is observed and assigned to organic fragments, for instance m/z = 26 ($C_2H_2^+$), 27 ($C_2H_3^+$) and 29 ($C_2H_5^+$) from the carbon black (in blue) and m/z = 31 (CF^+), 51 (CHF_2^+), 69 (CF_3^+), 77 ($C_3H_3F_2^+$) and 95 ($C_2H_2F_3^+$) from the PVdF binder (in green). The secondary ions characteristic of the LTO active material are also detected: m/z = 14 (Li_2^+), 48 (Ti^+), 49 (TiH^+), and 64 (TiO^+). The ionization process causes the formation of species like TiF^+ (m/z = 67) or TiO_3H^+ (m/z = 97) which come from the fragmentation of bigger molecules and/or re-arrangement of ions. Potassium (m/z=39), which has a high ionization yield, is also detected and attributed to surface contamination, coming from the chemical synthesis of the LTO powder.

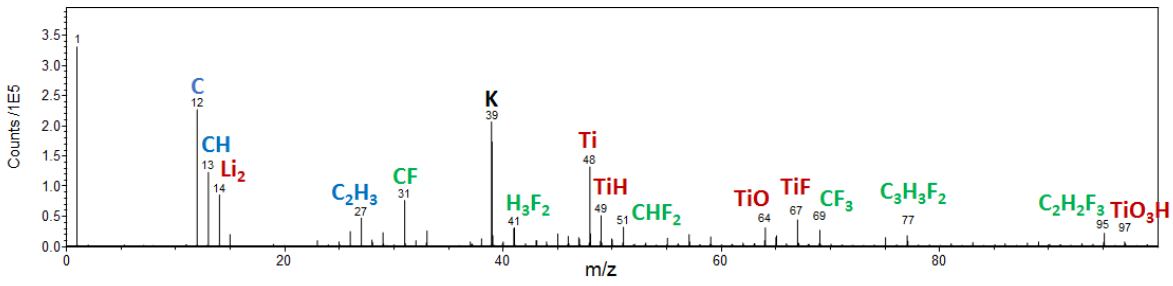

Figure 1. ToF-SIMS mass spectrum of the pristine LTO electrode over 0-100 m/z range in the positive polarity (blue, red and green peaks are attributed to carbon black, LTO active material and PVdF respectively). (in color)

3.1.2 Cycled LTO electrodes

Surfaces of LTO electrodes cycled facing either NMC or LMO electrodes were characterized after 1 and 100 cycles by ToF-SIMS (spectroscopic analysis and depth-profile experiments). Figure 2 presents the mass spectra obtained over 0-100 m/z range of cycled LTO negative electrode, after the first charge a), the first discharge b) facing NMC electrode, and after the

first charge c) and the first discharge d) facing LMO electrode. Note that potassium is detected for all cycled electrodes whatever the state of charge, but in lower proportion compared to the other peaks, due to its dissolution during the washing of cycled electrodes.

At the end of the first charge (figure 2a and 2c), the main positive secondary ion detected is Li_2F^+ fluorine species for both LTO electrodes facing NMC and LMO, which is characteristic of the SEI formation from $LiPF_6$ salt decomposition[26]. Organic species like carbonates or polymeric species m/z = 32 (CH_4O^+) and m/z = 59 ($C_4H_4Li^+$) related to the EC/EMC solvent degradation, are also detected but in lower proportion. Moreover, specific secondary ions m/z = 48 (Ti^+), m/z = 64 (TiO^+) of the LTO active material are still observed. Thus, ToF-SIMS evidences the covering process of the LTO electrodes by a thin (<5nm) and inhomogeneous (as the electrode compounds are still detected) surface layer since the first cycle, which is consistent with XPS results previously obtained in our group[22]. At the end of the first discharge, SEI fragments (Li_2F^+ and $C_4H_4Li^+$) are still visible on the mass spectra for the two systems but, the intensity of Ti^+ peak increases, which highlights the dissolution process of the surface layer formed upon charge, as already observed by XPS[22]. Note that this SEI dissolution phenomenon at the discharge state is partial; a passivation layer is still covering the surface of the negative electrode at the end of the first cycle, as similarly observed on graphite by Zhuo *et al*. using ToF-SIMS analysis[27]. Moreover, the ratio of the peaks intensities of Ti^+/Li_2F^+ and $Ti^+/C_4H_4Li^+$ are respectively lower for the electrode cycled facing LMO (0.2 and 0.8) than facing NMC (0.4 and 1.6). This suggests that the SEI at the LTO electrode cycled facing LMO is thicker than the one cycled facing NMC, which is once again consistent with our previous XPS results[22].

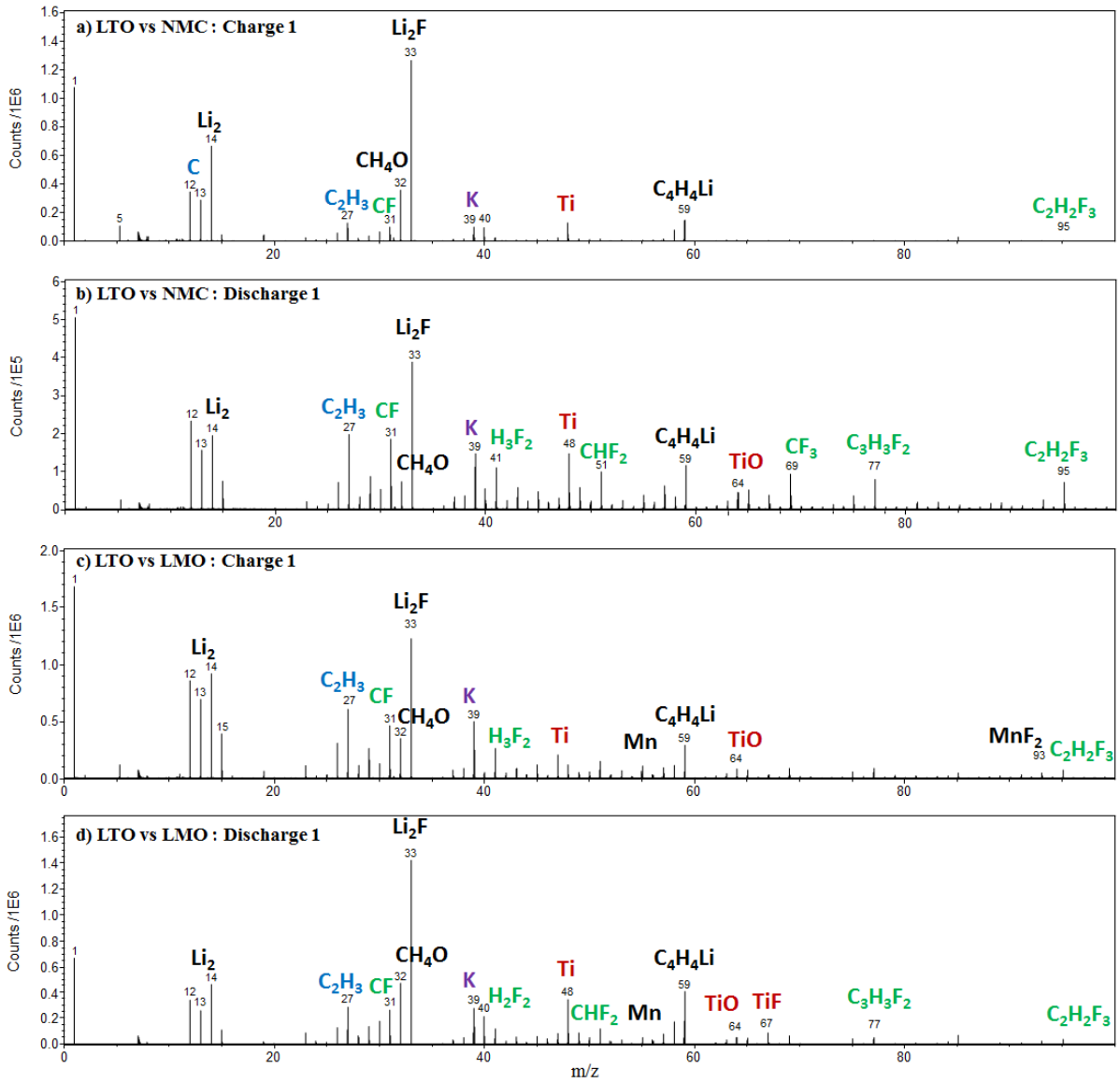

Figure 2. ToF-SIMS positive ion spectra over 0-100 m/z range for LTO electrodes cycled facing NMC after the first charge a), the first discharge b), and for LTO electrodes cycled facing LMO after the first charge c), and the first discharge d). (in color)

For the LTO/LMO system, manganese Mn^+ ion (fragment at m/z=55), is also detected in positive polarity at the surface of LTO electrodes since the first charge. This manganese comes from the LMO positive electrode dissolution and migrates through the electrolyte to the negative electrode during cycling. Due to the high sensitivity of ToF-SIMS, it is also possible to detect heavy metals (Ni^+, Mn^+ and Co^+) in low intensity at the LTO electrode surface facing NMC, coming from the NMC electrode dissolution during cycling (figure 3). Note that the detection of elemental metals in the ToF-SIMS positive spectrum is

mainly due to ionization process of SIMS, it does not mean they exist at the metallic state at the LTO electrode surface; these Mn^+, Ni^+ and Co^+ secondary ions are likely to come from molecules containing these metals, like MnF_2 for the LTO/LMO system, as suggested by XPS[22]. Indeed, this dissolution phenomenon of metals was already observed by XPS in our previous study for the LTO/LMO full cell but not for the LTO/NMC one. The number of counts for Mn^+ detected by ToF-SIMS at the LTO electrode surface cycled facing LMO is significant (around 2000 counts) whereas the one for LTO electrode cycled facing NMC is weaker (around 400 counts) so that it cannot be detected by XPS. These metals dissolution/migration processes are a proof of interactions between the two electrodes during cycling even for the LTO/NMC full cell. The presence of manganese in greater quantity over the LTO electrode surface vs LMO can destabilize the SEI and boost parasitic reactions at the electrode surface; which can entail the additional capacity loss observed for this system[19,22].

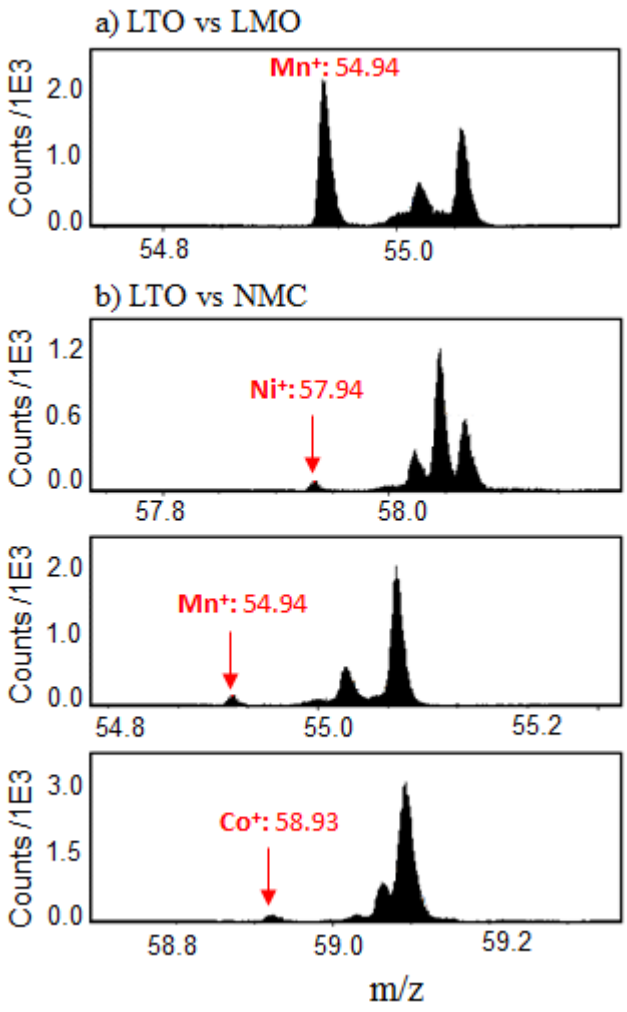

Figure 3. ToF-SIMS positive ion spectra of LTO electrodes cycled facing LMO a) and NMC b) after the first cycle over Mn^+, Ni^+, and Co^+ specific m/z ranges.

Interestingly, ToF-SIMS also reveals (figure S1) the presence of Titanium (coming from the LTO electrode dissolution) in low intensity at the positive electrode surfaces after cycling which is not possible to detect by XPS. Even if the formation of layers at the surface of positive electrodes had only a limited impact on the electrochemical performance of the systems in these conditions, this is another proof of interactions between electrodes: from the positive electrode to the negative one but also from the negative electrode to the positive one.

After the hundredth charge (figure S2), the same main fragments are detected for both systems at the LTO electrode surfaces as after the first charge: m/z = 14 (Li_2^+) and 33 (Li_2F^+) from $LiPF_6$ salt decomposition; 32 (CH_4O^+) and 59 ($C_4H_4Li^+$) from solvent degradation. At

the end of the 100th cycle, the intensity of the $C_4H_4Li^+$ peak is weaker compared to the 100th charge whereas the number of counts detected for the Ti^+ peaks increase on both electrodes, which is in agreement with the SEI dissolution process during discharge already observed at the first cycle. Moreover, the ratios Ti^+/Li_2F^+ and $Ti^+/C_4H_4Li^+$ are respectively lower for the LTO electrode cycled facing LMO (0.2 and 1.2) than for the one facing NMC (0.3 and 1.8), which is consistent with a thicker SEI layer for the LTO/LMO cell. Regarding the detection of Mn^+, it is still detected at the LTO electrode surface facing LMO after 100 cycles and in similar quantity than after one cycle; Ni^+, Co^+ and Mn^+ are also weakly detected on the LTO electrode surface facing NMC after 100 cycles. No difference in the amount of Mn-species on the LTO electrode (vs LMO) surface can be noticed on the ToF-SIMS spectra between charges and discharges and between the 1st and the 100th cycles. The concentration of Mn-species seems therefore independent of the charging state and it seems that most of the dissolved Mn is deposited since the first charge.

In order to have more information about Manganese and SEI species spatial distribution at the LTO electrode surfaces and because of the high in-depth resolution of ToF-SIMS, depth-profiles experiments (series of "analysis/sputtering" cycles) were performed after the first and the hundredth cycles for the two systems. No sputtering experiment has been performed on the pristine electrode as the objective is to analyze the 3D distribution of SEI specific species deposited at the LTO electrode surface during cycling. Figure 4 presents the concentration depth profiles of Ti^+ (representing the electrode active material, in blue), Li_2F^+ (representing inorganic SEI species, in green), $C_4H_4Li^+$ (representing organic SEI species, in yellow) and Mn^+ (in red) secondary ions obtained in the positive polarity for the LTO electrode cycled vs LMO after the first cycle, over 300 seconds of etching. Organic species ($C_4H_4Li^+$) concentration decreases quickly with the etching whereas a distinct rise of the bulk active material species (Ti^+) concentration is observed. Concerning LiF related species (Li_2F^+) and Manganese compounds, their concentration are gradually decreasing from

the extreme surface to the bulk of the electrode but with a "lower" concentration gradient than $C_4H_4Li^+$. Therefore, organic species are located mostly at the top surface of the LTO electrode while LiF and Manganese species are located both at the top surface and more deeply in the electrode surface layer, which is in agreement with a previous study by Nordh *et al.*[28].

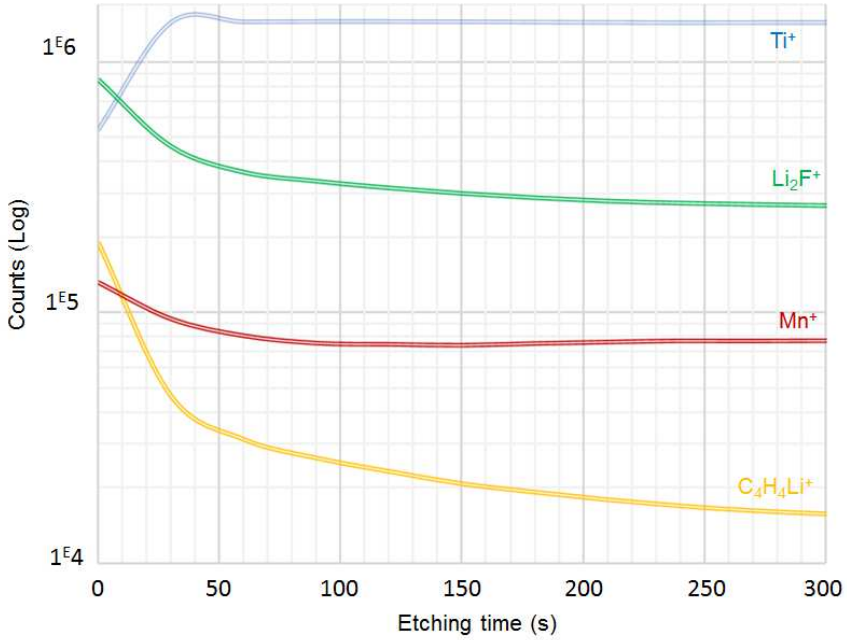

Figure 4. ToF-SIMS depth profiles of Ti^+ (blue), Li_2F^+ (green), Mn^+ (red) and $C_4H_4Li^+$ (yellow) secondary ions over 300 s etching time for the LTO/LMO system after the first cycle. (in color)

Figure 5 displays the 3D images reconstructed from depth-profile experiments performed in the positive polarity on LTO electrodes cycled vs NMC or LMO after one cycle and hundred cycles. The signal intensity of considered secondary ions (Ti^+, Li_2F^+, $C_4H_4Li^+$ or Mn^+) is plotted over the analyzed area (50µm x 50µm = x and y dimensions) versus the etching time (the z axis, 800s). For a better visibility, the z axis is over-dimensioned compared to the other axes. Each species has a 3D spatial distribution over the analyzed volume with one specific color (Ti^+ in blue, Li_2F^+ in green, $C_4H_4Li^+$ in yellow and Mn^+ in red). When a color is not appearing anymore on the image, it means the signal intensity of the

secondary ion is too low in the mass spectrum to be plotted. The final 3D map corresponds to the overlay of all 3D spatial distributions of the considered species. Note that it was not possible to reconstruct the 3D spatial distribution of Mn^+, Co^+ and Ni^+ secondary ions detected on the LTO electrode surface cycled facing NMC as their signal intensities in the mass spectra were too weak.

After the first cycle for the LTO/LMO system, organic species (in yellow) are located exclusively at the top surface of the electrode while LiF related species (in green) and Manganese (in red) are present both at the extreme surface and more deeply in the electrode surface layer. The same trend is observed for the LTO electrode cycled facing NMC, organic species (in yellow) are accumulated only at the top of the electrode surface, whereas LiF compounds diffuse more in the surface layer. Moreover, LiF species seem to insert deeper in the SEI of LTO electrode facing LMO than in the one of LTO electrode facing NMC after one cycle. Concerning organic species, their 3D spatial distribution seems more inhomogeneous over the LTO electrode surface cycled facing LMO than facing NMC, which can be explained by the presence of manganese inducing a destabilization of the SEI and a decrease of electrochemical performances of LTO/LMO cells. On the contrary, the SEI of LTO/NMC cells seems more protective (organic compounds are homogeneously spread over the surface) which is in good agreement with the coulombic efficiency evolution, indicating the passivation of the LTO electrodes (vs NMC) since the first cycle.

After the hundredth cycle, organic species are still mostly concentrated at the top surface of the LTO electrode for both systems. Note that for LTO/LMO cells, organic species are spread more homogeneously all over the LTO electrode surface compared to the first cycle, which could be related to a surface structural rearrangement and a stabilization of the SEI after long cycling, meaning a better passivation of the LTO electrode in correlation with a stabilization of the capacity[22,26,28]. 3D imaging also evidences that a greater amount of LiF inserts deeper within the SEI of the LTO electrode after hundred cycles than after the first

cycle. Regarding the signal of $^{55}Mn^{+}$, its profile after 100 cycles is very similar to the one after the first cycle: it is gradually decreasing from the extreme surface layer to the inner of the SEI, which confirms that Manganese deposition mainly occurs at the first cycle. For LTO/NMC system, organic compounds are still mainly located at the extreme surface after hundred cycles, meaning a stable SEI correlated with a stable capacity, while LiF related species insert more deeply into the SEI of the LTO electrode after 100 cycles than after one cycle, like for LTO/LMO cells. However, more LiF related species are formed for LTO/LMO cells than for LTO/NMC ones after 100 cycles, which can be related to the longer time spent at a higher potential, degrading more $LiPF_6$ salt and producing LiF in greater proportion, which is consistent with a ticker SEI for the LTO/LMO system.

Several hypothesis can be mentioned to explain why LiF is found in the inner part of the SEI for both systems: as suggested by Nordh et al[28], it is the first one to be formed from $LiPF_6$ salt degradation, but the presence of LiF both at the extreme surface and deeply in the SEI during all the cycling suggests that part of LiF may be formed elsewhere, particularly at the positive electrode surface; LiF related species then diffuse through the electrolyte to be finally deposited on the LTO electrode surface. Moreover, the smaller size of LiF related species compared to organic ones can also play a role in their spatial distribution into the SEI.

Consequently, these ToF-SIMS experiments highlight that salt degradation products (mostly LiF) and active materials dissolution species (Mn, Ni and Co) are also produced at the positive electrodes and then migrate to the negative electrodes surface where they are either reduced or simply deposited. These degradation phenomena seem to be accelerated at high voltage (here for LMO electrode) which is in agreement with the results of Madec *et al.*[29].

In order to complement and confirm the previous ToF-SIMS results, XPS analysis were performed using two different incident photons beams, either Al (1486.6 eV, depth of analysis of 5-10 nm) or Ag (2984.3 eV, depth of analysis of 10-20 nm), so that to obtain

chemical information at the top of the electrode surface (with Al source) and deeper into the electrode (with Ag source).

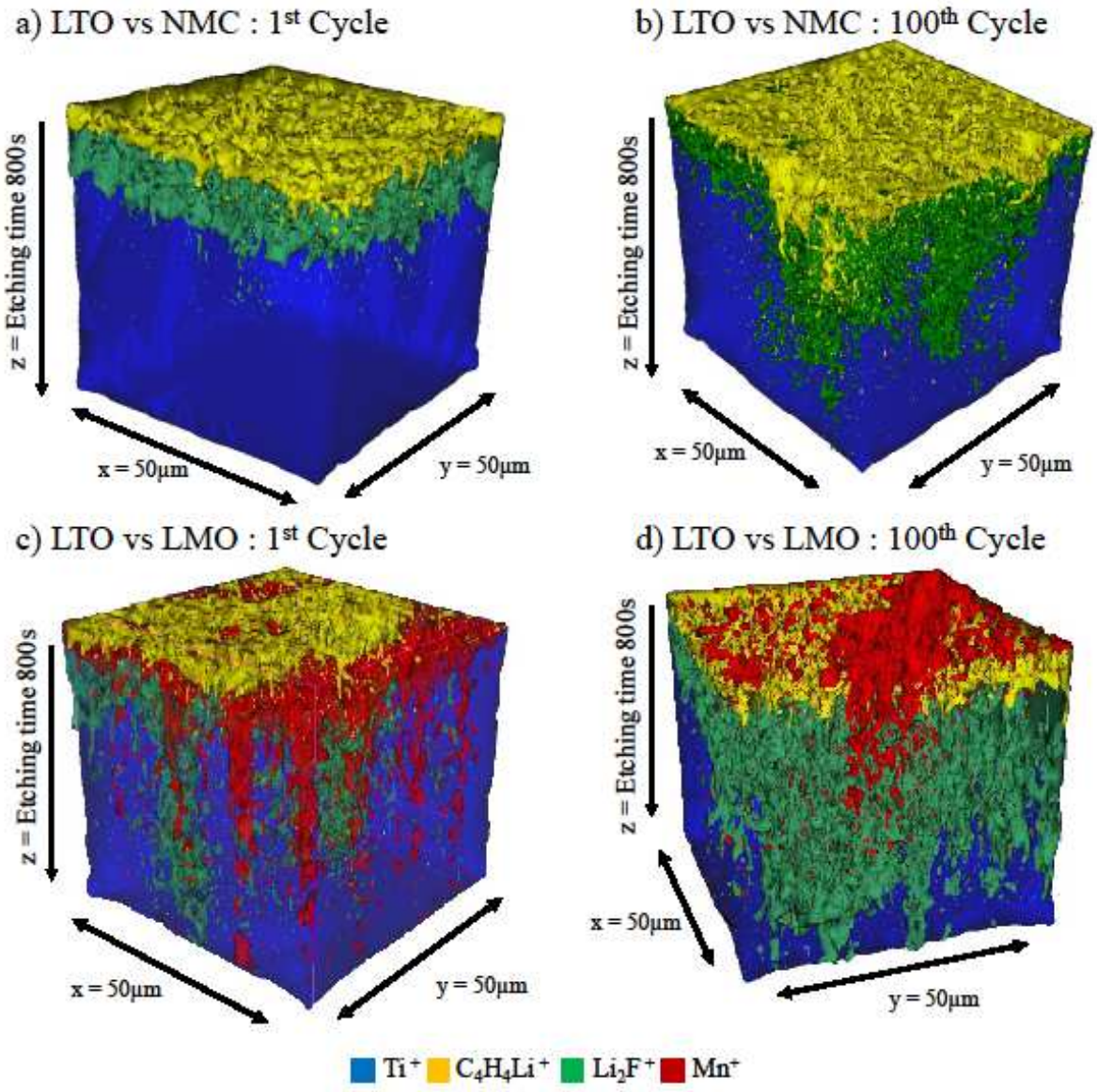

Figure 5. 3D images reconstruction from ToF-SIMS depth profile experiments showing the spatial distributions of Ti^+, $C_4H_4Li^+$, $Li_3F_2^+$ and Mn^+ secondary ions over 50µm (x axis) by 50µm (y axis) raster size and 800s etching time (z axis), at the LTO electrodes surfaces at the end of the first and the hundredth cycles versus NMC electrode a) and b) and versus LMO electrode c) and d). (in color)

3.2 XPS analysis

Figure 6 presents C 1s a), O 1s b) and F 1s c) XPS core peaks of cycled LTO negative electrodes in front of LMO electrode at the end of the first cycle obtained with the two sources (XPS spectra of LTO electrodes cycled versus NMC are reported in the supporting information, figure S4). With Al Kα radiation (first line), the analysis of C 1s spectra shows the formation of new organic species at the electrode surface at the end of the first cycle. Indeed, in addition to the components characteristics of the pristine electrode (carbon black at 283.9 eV in blue, **C**H_2 at 286.2 eV, **C**F_2 at 290.7 eV and **C**F_3 at 292.1 eV from the PVdF binder in green[11]), the appearance of C 1s components at 286.7 eV, 287.8 eV and 289.2 eV attributed respectively to **C**-O, **C**=O and O=**C**-O/**C**O_3^{2-} chemical environments are observed. Similarly, three O 1s components at 531.6 eV (**O**=C-O or C–**O**–Li chemical environments), 533.0 eV (**O**=C or C–**O**–C) and 534.0 eV (**O**–P) can also be detected on the LTO electrode surface[21,29] in addition to the LTO component at 530.0 eV (in red). This evidences the covering process of the electrode by a surface layer (SEI) from the deposition of new species, namely oxalates, poly(ethylene oxide) (PEO), $EtOCO_2Li$ and phosphates ((PO_4^{3-}) or $PO(RO)_3$). On the F 1s spectrum, an intense component at 685.2 eV (light gray) corresponding to LiF and a second less intense component at 686.3 eV (dark gray) corresponding to fluorophosphates ($Li_xPO_yF_z$) deposited at the surface of the electrode are observed in addition to the most intense peak at 687.8 eV corresponding to C**F**$_2$ of the PVdF (green)[22,30]. All these results confirm the degradation process of the electrolyte $LiPF_6$ salt and the solvent after the first cycle and the deposition of related species at the surface of the negative electrode. With Ag Lα radiation (second line), the SEI components are still visible on the O 1s spectrum but in lower relative intensity than with Al Kα radiation, which confirms that organic species are mainly located at the LTO electrode surface. This is accompanied by a decrease of C-C/C-H (from surface contamination and SEI species)

component intensity at 285.0 eV on the C 1s spectrum (from 19.1% to 12.3%). However, regarding F 1s spectra, LiF is in greater proportion than CF_2 component with Ag source (34% compared to 20% with Al source), which means LiF species are present deeper in the LTO electrode surface layer than the other SEI species, which is consistent with ToF-SIMS depth-profile results.

Note that with Al source, quantification is carried out using Scofield's relative sensitivity factors[31] whereas with Ag source, the choice was made to calculate only the relative percentages (% reported in figure 6) which are sufficient to qualitatively compare the evolution of the different components in spectra. Atomic concentrations (at. %) of the different chemical environments identified by XPS with Al source at the surface of the cycled LTO electrodes are reported in Table S1.

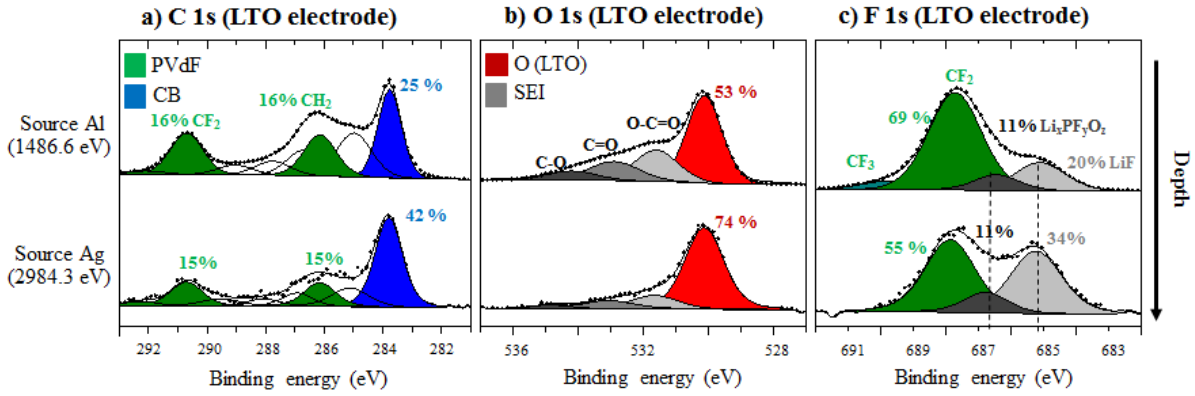

Figure 6. C 1s a), O 1s b) and F 1s c) XPS spectra of cycled LTO negative electrodes at the end of the first cycle in front of LMO electrode obtained with Al Kα radiation (hν=1486.6 eV) (first line) and Ag Lα radiation (hν=2984.3 eV) (second line). The relative percentages of main components are reported in the figure. (in color)

At the end of the hundredth cycle (spectra in supporting information, figure S3 and S5), similar organic SEI species (C-O, C=O and **O**=C-O/CO_3) are detected in C1s and O1s spectra at the LTO electrode surface than after the first cycle with Al source, but in greater

quantities which proves the growth of the SEI thickness over cycling. With Ag source, the intensity of these components decreases which proves that organic species are still mainly located on top of the LTO electrode surface after the hundredth cycle like after the first one. Concerning fluorine species, the ratio between CF_2 and LiF peaks is independent of the number of cycles but it is greater when the depth of analysis is deeper. This result proves again that LiF diffuses into the SEI upon cycling, which is in agreement with ToF-SIMS results.

Finally, titanium, carbon, oxygen and fluorine species from LTO electrode active material are detected with Al source during all the cycling which proves that the thickness of the interfacial layer is lower than 10 nm for both systems as the XPS analysis depth is about 5-10 nm. Moreover, considering the 10-20 nm analysis depth of XPS with Ag source, this result allows estimating the ToF-SIMS sputtered depth (figures 4 and 5) between 20 nm and 30 nm, as Ti^+ active material (in blue) is detected in majority at the end of the etching.

4. CONCLUSIONS

LTO electrodes cycled facing either LMO or NMC were characterized by ToF-SIMS (surface analysis, depth-profile experiments and 3D image reconstruction) and XPS using 2 different sources (Al and Ag), which gives new insights on the in-depth distribution of SEI species over cycling and proves the consistency of the results obtained with these two techniques.

For both systems, it was found that organic SEI species are located exclusively at the top surface of the electrode whereas inorganic compounds like LiF are present both at the top of the surface layer and more deeply into it since the first cycle; this insertion of LiF within the SEI of the electrode is even more pronounced after 100 cycles. Moreover, Manganese is detected at the LTO electrode surface cycled vs LMO as well as deeply into the surface layer

since the first cycle and its proportion does not seem to evolve with cycling; this proves the dissolution of the manganese at the LMO electrode, its migration through the electrolyte and its deposition and insertion into the SEI formed at LTO electrode during the first cycle. Furthermore, the trace-sensitivity of ToF-SIMS also allows to detect small amounts of Ni, Mn and Co metals at the LTO electrode cycled facing NMC, as well as low amount of titanium at the LMO or NMC electrodes, which confirms the interactions between negative and positive electrodes during cycling.

The presence of manganese compounds and the formation of a thicker layer on the anode facing LMO than facing NMC, especially due to greater quantities of fluorinated species entering deeply in the SEI, can impede the diffusion of lithium and explain the decrease of the retention capacity for the LTO/LMO system. Overall, even if $LiPF_6$ salt may be the first compound to degrade, our ToF-SIMS results highlight for the first time failure mechanisms which seem to be driven by oxidative parasitic reactions at the positive electrode and interactions with the negative one. To go further into this study, other types of salts like for instance $LiClO_4$ could be tested[32].

Finally, this study proves that ToF-SIMS, thanks to its high sensitivity and high in-depth resolution, is well adapted to characterize very thin surface layers commonly found at the electrolyte/electrode interfaces, whose properties greatly influence batteries electrochemical performances. Consequently, ToF-SIMS is a very promising analysis tool in the field of battery science, as a complement to XPS technique.

ACKNOWLEDGEMENTS

The work was supported by funding from The French National Research Agency via the project ANR-11-EQPX-0027 MARSS and SAFT company.

Competing financial interests

The authors declare that they have no competing financial interest.

REFERENCES

[1] Goodenough, J. B.; Kim, Y. Challenges for rechargeable Li batteries. *Chem. Mater.* **2010**, 22, 587–603.

[2] Wu, K.; Yang, J.; Zhang, Y.; Wang, C.; Wang, D. Investigation on $Li_4Ti_5O_{12}$ Batteries Developed for Hybrid Electric Vehicle. *J.Appl. Electrochem.* **2012,** *42* (12), 989-995.

[3] Peled, E.; Golodnitsky, D.; Ardel, G. Advanced Model for Solid Electrolyte Interphase Electrodes in Liquid and Polymer Electrolytes. *J. Electrochem. Soc*., Vol. 144, No. **8,** August **1997**

[4] E. Peled and S. Menkin. Review, SEI: Past, Present and Future. *Journal of The Electrochemical Society*, **164** (7) A1703-A1719 (2017)

[5] Goodenough, J. B. The Li-Ion Rechargeable Battery: A Perspective. *Journal of the American Chemical Society* **2013**, 135 (4), 1167–1176.

[6] Chen, Z.; Li, H.; Wu, L.; Lu, X.; Zhang, X. $Li_4Ti_5O_{12}$ Anode: Structural Design from Material to Electrode and the Construction of Energy Storage Devices. Chem. Rec. **2017**, 17, 1–32.

[7] Ohzuku, T. Zero-strain insertion material of $Li[Li_{1/3}Ti_{5/3}]O_4$ for rechargeable lithium cells. *Journal of the Electrochemical Society* **1995**, 142, no. 5: 1431–35.

[8] Zaghib, K.; Simoneau, M.; Armand, M.; Gauthier, M. Electrochemical study of $Li_4Ti_5O_{12}$ as negative electrode for Li-ion polymer rechargeable batteries. *Journal of Power Sources* 81–82, 1999. 300–305.

[9] El Ouatani, L.; Dedryvère, R.; Siret, C.; Biensan, P.; Reynaud, S.; Iratçabal, P.; Gonbeau, D. The effect of vinylene carbonate additive on surface film formation on both electrodes in Li-Ion batteries, *J. Electrochem. Soc.* **2009**, 156 (2), A103.

[10] Dedryvère, R.; Foix, D.; Franger, S.; Patoux, S.; Daniel, L.; Gonbeau, D. Electrode/Electrolyte Interface Reactivity in High-Voltage Spinel $LiMn_{1.6}Ni_{0.4}O_4/Li_4Ti_5O_{12}$ Lithium-Ion Battery. *The Journal of Physical Chemistry C* **2010**, *114*, 10999–11008.

[11] Song, M.-S.; Kim, R.-H.; Baek, S.-W.; Lee, K.-S.; Park, K.; Benayad, A. Is $Li_4Ti_5O_{12}$ a solid-electrolyte-interphase-free electrode material in li-ion batteries? Reactivity between the $Li_4Ti_5O_{12}$ electrode and electrolyte, *Journal of Materials Chemistry* A **2014**, 2 (3), 631-636.

[12] Gieu, J.-B.; Courrèges, C.; El Ouatani, L.; Tessier, C.; Martinez, H. Temperature effects on $Li_4Ti_5O_{12}$ electrode/electrolyte interfaces at the first cycle: A X-ray Photoelectron Spectroscopy and Scanning Auger Microscopy study. *Journal of Power Sources* **2016**, *318*, 291–301.

[13] Gieu, J.-B.; Courrèges, C.; El Ouatani, L.; Tessier, C.; Martinez, H. Influence of Vinylene Carbonate additive on the $Li_4Ti_5O_{12}$ electrode/electrolyte interface for lithium-ion batteries. *Journal of the Electrochemical Society* **2013**, 164(6) A1314-A1320.

[14] Wu, K.; Yang, J.; Liu, Y.; Zhang, Y.; Wang, C.; Xu, J.; Ning, F.; Wang, D. Investigation on gas generation of $Li_4Ti_5O_{12}$/$LiNi_{1/3}Co_{1/3}Mn_{1/3}O_2$ cells at elevated temperature. *Journal of Power Sources* 237 (**2013**) 285-290.

[15] Wang, Q.; Zhang, J.; Liu, W.; Xie, X.; Xia, B. Quantitative investigation of the gassing behavior in cylindrical $Li_4Ti_5O_{12}$ batteries. *Journal of Power Sources* 343 (2017) 564-570.

[16] Chancelier, L.; Benayad, A.; Gutel, T.; Mailley, S.; Santinia, C. C. Characterization of LTO//NMC Batteries Containing Ionic Liquid or Carbonate Electrolytes after Cycling and overcharge. *Journal of The Electrochemical Society*, 162 (6) A1008-A1013 (2015).

[17] Belharouak, I.; Koenig, G. M.; Amine, K. Electrochemistry and safety of $Li_4Ti_5O_{12}$ and graphite anodes paired with $LiMn_2O_4$ for hybrid electric vehicle Li-ion battery applications. *Journal of Power Sources* **2011**, 196(23) :10344–10350.

[18] Joshi, T.; Eom, K.; Yushin, G.; Fuller, T. F. Effects of Dissolved Transition Metals on the Electrochemical Performance and SEI Growth in Lithium-Ion Batteries. *Journal of The Electrochemical Society*, 161 (12) A1915-A1921 (**2014**).

[19] Wu, K.; Qian, L.; Sun, X.; Wu, N.; Zhao, H.; Zhang, Y. Influence of manganese ions dissolved from $LiMn_2O_4$ cathode on the degradation of Li4Ti5O12-based lithium-ion batteries. J Solid State Electrochem. (2017).

[20] Gilbert, J.; Shkrob, I.; Abraham, D. Transition Metal Dissolution, Ion Migration, Electrocatalytic Reduction and Capacity Loss in Lithium-Ion Full Cells. *Journal of The Electrochemical Society* (**2017**), 164(2) A389-A399.

[21] Gieu, J.-B.; Courrèges, C.; El Ouatani, L.; Tessier, C.; Martinez, H. New insights in the characterization of the electrode/electrolyte interfaces within $LiMn_2O_4$/$Li_4Ti_5O_{12}$ cells, by X-ray

Photoelectron Spectroscopy, Scanning Auger Microscopy and Time-of-Flight Secondary Ions Mass Spectrometry. *Journal of material Chemistry A*, **2017**, 5, 15315-15325.

[22] Gauthier, N.; Courrèges, C.; Goubault, L.; Demeaux, J.; Tessier, C.; Martinez, H. Influence of the Positive Electrode on Li4Ti5O12 (LTO) Electrode/Electrolyte Interfaces in Li-Ion Batteries. *Journal of The Electrochemical Society* (**2018**), 165 (13) A2925-A2934.

[23] Vissers, D. R.; Chen, Z.; Shao, Y.; Engelhard, M.; Das, U.; Redfern, P.; Curtiss, L. A.; Pan, B.; Liu, J.; Amine, K. Role of Manganese Deposition on Graphite in the Capacity Fading of Lithium Ion Batteries. ACS Appl. Mater. Interfaces 2016, 8, 14244−14251.

[24] Peng Lu, Chen Li, Eric W. Schneider, Stephen J. Harris. Chemistry, Impedance, and Morphology Evolution in Solid Electrolyte Interphase Films during Formation in Lithium Ion Batteries. J. Phys. Chem. C 2014, 118, 896−903.

[25] Busche, M. R.; Drossel, T.; Leichtweiss, T.; Weber, D. A.; Falk, M.; Schneider, M.; Reich, M-L.; Sommer, H.; Adelhelm, P.; Janek, J.Dynamic formation of a solid-liquid electrolyte interphase and its consequences for hybrid-battery concepts. Nature Chemistry 2016, 8.

[26] Daigle, JC.; Asakawa, Y.; Hovington P.; Zaghib, K. Schiff Base as Additive for Preventing Gas Evolution in $Li_4Ti_5O_{12}$-Based Lithium-Ion Battery. *ACS Appl. Mater. Interfaces*. 2017 Nov 29;9(47):41371-41377.

[27] Zhuo, Z.; Lu, P.; Delacourt, C.; Qiao, R.; Xu, K.; Pan, F.; Harris, S. J.; Yang, W. Breathing and oscillating growth of Solid-electrolyte-interphase upon electrochemical cycling. *Chem. Commun.,* 2018, 54, 814—817.

[28] Nordh, T.; Younesi, R.; Brandell, D.; Edström, K. Depth profiling the solid electrolyte interphase on lithium titanate ($Li_4Ti_5O_{12}$) using synchrotron-based photoelectron spectroscopy. Journal of Power Sources 294 (2015) 173-179.

[29] Madec, L.; Ellis, L. D. Exploring Interactions between Electrodes in Li[NixMnyCo1-xy]O_2/Graphite Cells through Electrode/Electrolyte Interfaces Analysis**.** *Journal of The Electrochemical Society*, **164** (14) A3718-A3726 (**2017**).

[30] Verma, P.; Maire, P.; Novák, P. A review of the features and analyses of the solid electrolyte interphase in Li-ion Batteries. *Electrochimica Acta* 55 (2010) 6332–6341.

[31] J.H. Scofield, Hartree-Slater subshell photoionization cross-sections at 1254 and 1487 eV, J. Electron Spectros. Relat. Phenomena. 8 (1976) 129–137.

[32] J.M. Tarascon, D. Guyomard, New electrolyte compositions stable over the 0 to 5 V voltage range and compatible with the $Li_{1+x}Mn_2O_4$/carbon Li-ion cells, Solid State Ionics, 69 (1994) 293-305.

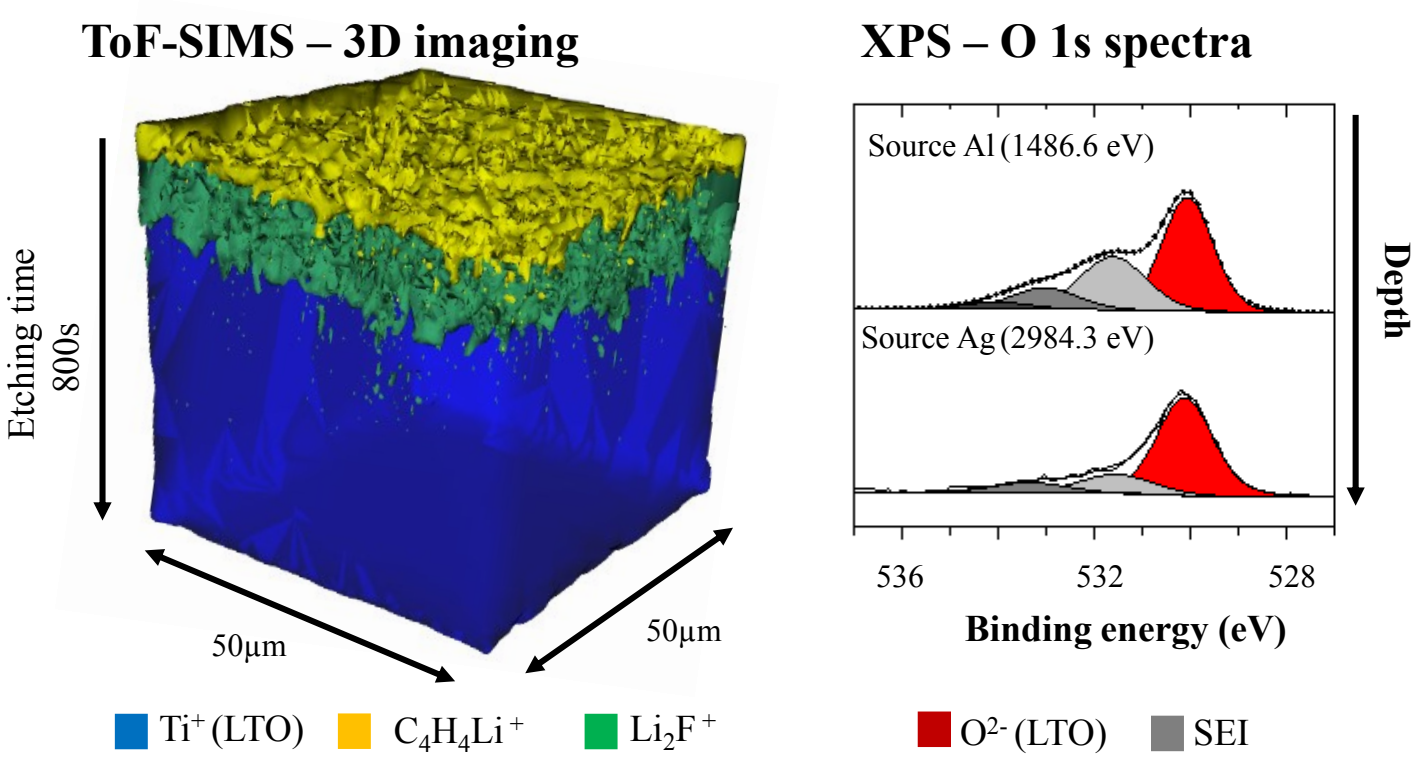

LTO electrode – 1st cycle